3. Soft X-Ray Observations

Experiment MA-048

S. Shulman,[a] S. Naranan,[ab] W. Snyder,[c] D. Yentis,[a] R. Cruddace,[a] H. Friedman,[a†] G. Fritz,[a] and R. Henry[c]

ABSTRACT

The Soft X-Ray Experiment was designed to observe celestial X-ray sources in the energy range from 0.1 to 10 keV. The X-ray spectra and fast-time variability were measured to characterize the emission from a number of such sources. A new X-ray pulsar was discovered, and a new X-ray-emitting supernova remnant was detected.

OBJECTIVES

The objectives of the Apollo-Soyuz Test Project (ASTP) Soft X-Ray Experiment were to study the spectra of a large number of known celestial X-ray sources in the range from 0.1 to 10 keV, to search for periodicities and other variability in these sources, and to more precisely map the soft X-ray diffuse background. Celestial X-ray sources have been observed from rockets and satellites for approximately a decade, and more than 200 sources have been located. Figure 3-1 is a map of the sky in galactic coordinates showing the sources located by the *Uhuru* small astronomy satellite (SAS-1). The concentration in the galactic plane indicates a class of sources within the galaxy, and the uniform distribution at high latitudes indicates a class of extragalactic objects.

The objective of spectral measurements in the range from 0.1 to 10 keV is twofold. First, detailed comparison of the spectra of many sources would provide the capability to classify X-ray sources more precisely in terms of the X-ray emission mechanism and the relevant physical parameters such as size, density, temperature, magnetic field strength, and relativistic particle content. Second, the low-energy parts of the spectra (less than 2 keV) are affected by absorption in the intervening interstellar material. A measure of the absorption can be used to establish a fairly precise distance scale for the X-ray sources. The distances in turn yield the absolute luminosities and the relationship to other features of galactic structure such as the spiral arms.

The search for periodicities and fast-time variability was conducted by recording the counts in 3-millisecond intervals for three broad energy bands. The objective was to search for new pulsars (presumably rotating neutron stars) and for other types of sources where intensity variations on a fast-time scale might provide information on the source structure, size, and emission mechanisms.

The third objective of the experiment was to map the soft X-ray background. At energies of approximately 0.25 keV, there is an observable diffuse emission from all directions in the sky. Figure 3-2 is a map obtained from data taken during an Aerobee rocket flight. To map a significant portion of the sky during the 5-minute flight, a wide field of view (10° by 10°) and a rapid scan rate were used. As a result, the statistical precision of the map is poor, and the minimum contrast features that can be detected are quite bright. The increased observing time available with the ASTP instrument provided the opportunity to use a 4°

[a]Naval Research Laboratory.

[b]On leave from Tata Institute of Fundamental Research, Bombay, India.

[c]Johns Hopkins University.

[†]Principal Investigator.

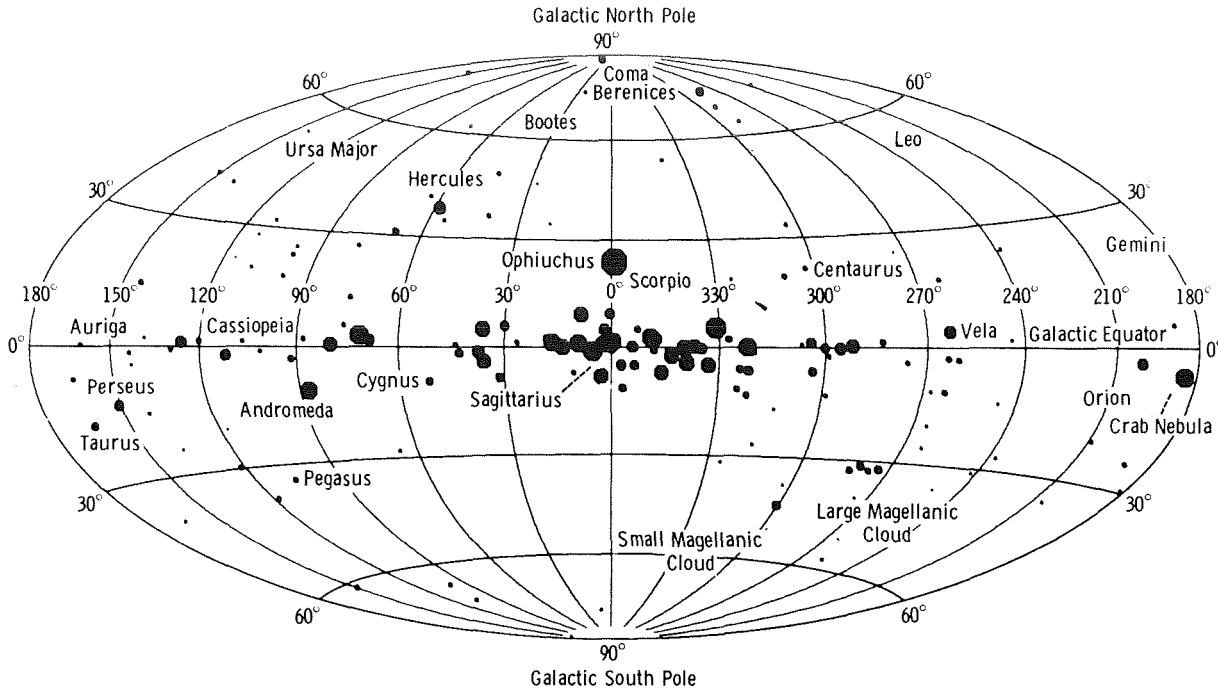

FIGURE 3-1.—Map of 2- to 10-keV X-ray sources as determined by the *Uhuru* satellite.

by 4° field of view and to obtain approximately 10 times as much data in each resolution element. With increased resolution, an attempt is being made to determine the origins of the soft X-ray diffuse background.

INSTRUMENT DESCRIPTION

The X-ray instrument is a large-area proportional counter very similar to those that have been flown on sounding rockets by several groups. The proportional counter detects individual X-ray photons when they interact in the detector gas. This interaction produces photoelectrons that drift toward a high-voltage anode and produce secondary electrons. In the high electric field region near the anode, the secondary electrons initiate an electron avalanche, which produces an electronic pulse that can easily be amplified and detected. In the proportional counter (as opposed to the Geiger counter), the total charge in the avalanche pulse is proportional to the original number of secondary electrons; thus, information about the energy of the detected X-ray is preserved.

The detector gas is a standard mixture of 90 percent argon and 10 percent methane (P10 gas) at 110 kN/m^2 (1.1 atm). The detector anodes are nominally operated at 2700 V, and the instrument contains a feedback system to adjust this voltage to keep the gain constant during variations in detector temperature. The gas is contained by a 2-μm polycarbonate window that requires an elaborate support structure to withstand the 110-kN/m^2 (1.1 atm) pressure. This thin window is necessary to permit the detection of X-rays in the 0.1- to 2-keV energy range: these X-rays would be absorbed by more conventional window materials such as 50-μm beryllium. Aluminum honeycomb is part of the window support structure and also provides the instrument collimation that gives a circular field of view with a full-width half-maximum (FWHM) response of 4°. The effective area for X-ray detection is 1200 cm^2. The front face of the detector, including the honeycomb and support ribs, is shown in figure 3-3.

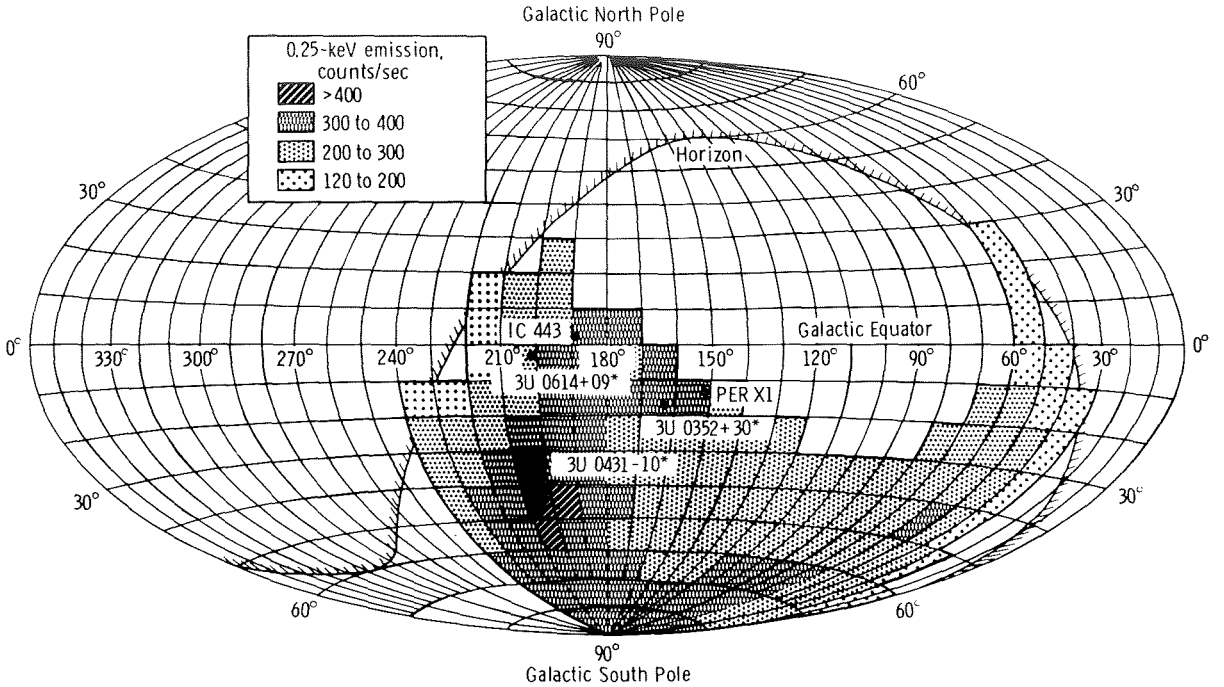

*Source designations from the Uhuru catalog.

FIGURE 3-2.—Map of diffuse 0.25-keV X-ray emission from a Naval Research Laboratory (NRL) rocket observation.

Because a thin window is required for the low-energy X-ray observations, a gas supply is required to replenish gas that escapes through small pinholes in the window. Typical leak rates into vacuum range from 10 to 100 cm^3 Pa/min (10 to 100 cm^3 atm/min). A 30.5-cm (12 in.) diameter reservoir tank was incorporated into the experiment and was pressurized to 17 000 kN/m^2 (170 atm) approximately 35 days before launch. With this gas supply system, the detector could also be completely emptied and refilled by astronaut command to remove atmospheric contaminants that diffused into the detector before launch. The gas tank is a prominent feature in the rear view of the instrument shown in figure 3-4.

The electronic design of the instrument is shown in figure 3-5. There are two sets of anodes in the detector, one for X-ray data and one for the veto of charged particles. Each set has a separate preamplifier and discriminator. A data pulse is accepted and analyzed only if no pulse is detected within a few microseconds in the veto section. Data pulses that are accepted are then pulse height analyzed, and the pulse height is stored for telemetry readout. The analysis is accomplished by a 9-bit analog-to-digital (A-D) converter that uses a successive approximation scheme. Each pulse height is also sorted into one of three energy bins for accumulation in the 3-microsecond fast-timing bins. The electronics are mounted on the rear of the detector as shown in figure 3-4.

The crucial parameters of gain and resolution were measured during laboratory calibrations. These parameters are required to determine the spectrum of X-rays incident on the detector. The detector response is convolved with the incident photon spectrum to give the counts observed in each pulse-height bin of the spectral data. Mathematically, this is described as follows:

$$N(V_1,V_2) = \int_{E_1=G(V_1)}^{E_2=G(V_2)} dE \int_0^\infty T(E')\, A(E')\, R(E',E)\, N(E')\, dE' \qquad (3\text{-}1)$$

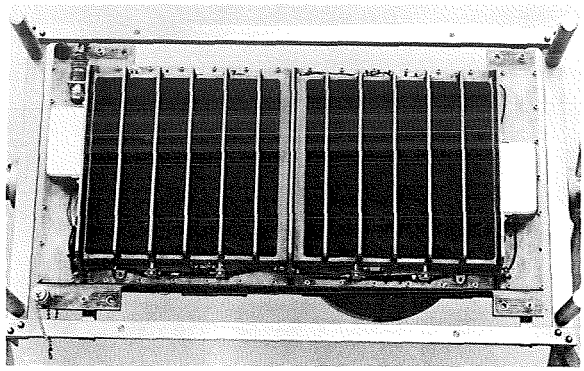

FIGURE 3-3.—Front view of the ASTP X-ray detector.

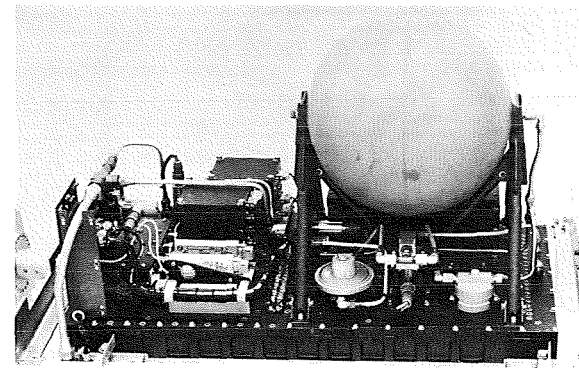

FIGURE 3-4.—Rear view of the ASTP X-ray detector with the electromagnetic interference shield removed.

where N is the counting rate, V_1 and V_2 are the boundaries of the pulse-height channel, $T(E')$ is the window transmission as a function of energy, $A(E')$ is the gas absorption as a function of energy, $R(E',E)$ is the resolution function, $N(E')$ is the incident photon spectrum, and $G(V)$ is the pulse-height gain function. The functions T and A can be calculated from measurements made at a number of different laboratories. The gain $G(V)$ and the resolution function $R(E',E)$ are determined by laboratory calibrations with monochromatic X-rays incident on the detector. The peak in the spectral data yields the gain, and the shape of the spectral data yields the resolution function. At most energies, the resolution function is Gaussian; however, at low energies, a Poisson function gives a better fit because the parameters must all be greater than zero.

The gain calibration is given in figure 3-6. Energy is plotted as a function of channel number rather than channel voltage. The instrument gain is linear to within 10 percent over the entire range from 0.1 to 8 keV. A significant nonlinearity of approximately 10 percent is noticeable at the higher energies. The resolution function averaged over the entire sensitive area of the detector at an

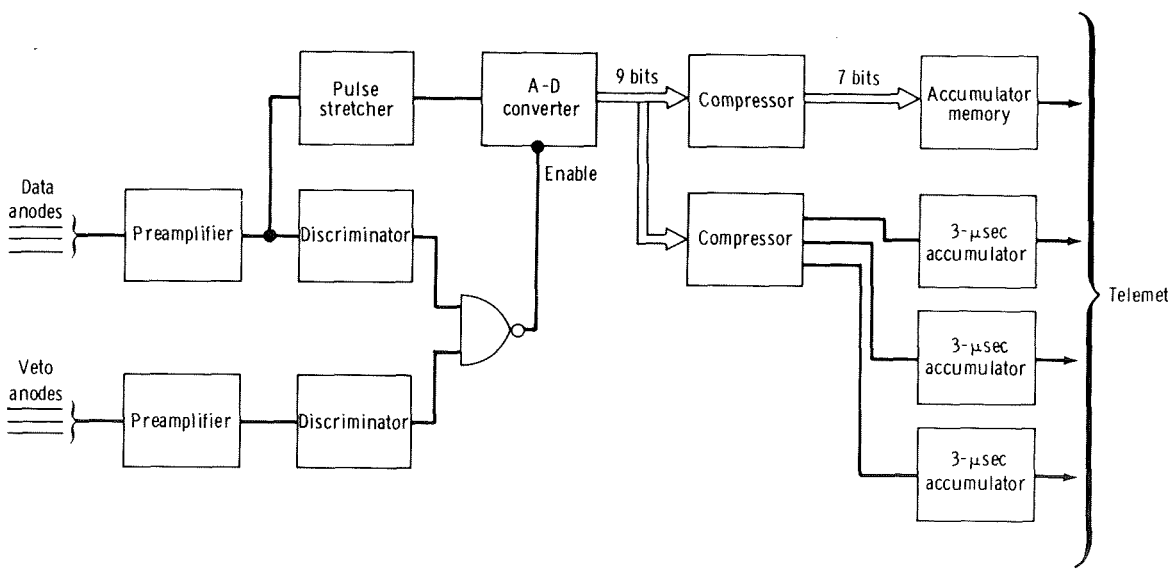

FIGURE 3-5.—Simplified block diagram of the detector electronics.

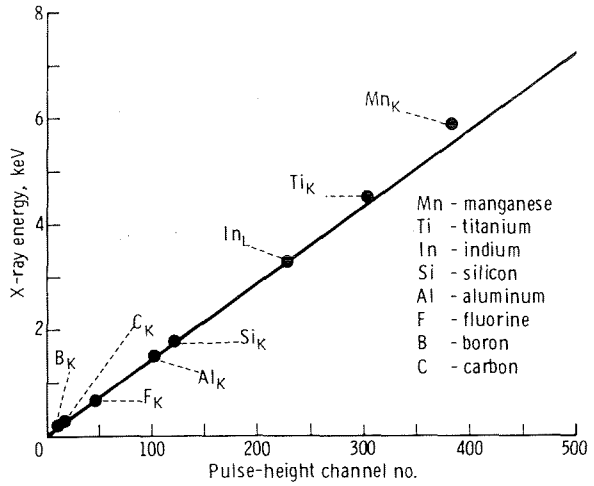

FIGURE 3-6.—Laboratory gain calibration of the ASTP detector.

energy of 5.98 keV (Mn_K) is shown in figure 3-7. The FWHM of the function is approximately 27 percent. The FWHM at any single point in the detector is considerably better (approximately 20 percent), but slight gain variations from point to point broaden the average resolution. The FWHM resolution is plotted as a function of energy in figure 3-8.

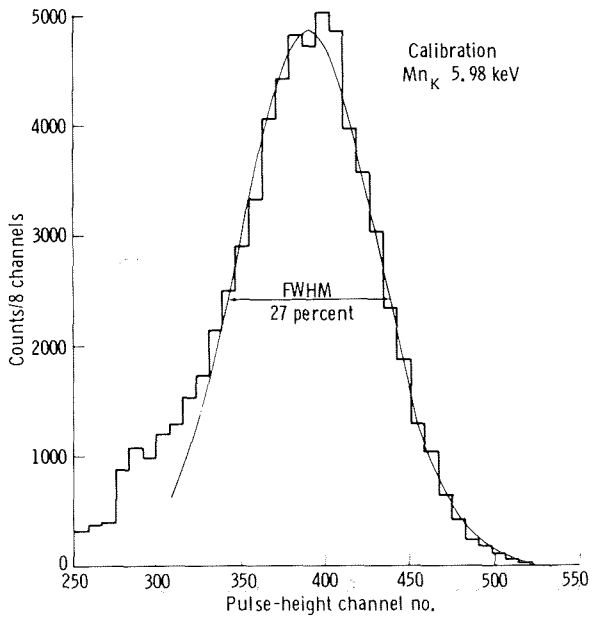

FIGURE 3-7.—Laboratory calibration spectrum of the Mn_K X-ray line at 5.98 keV.

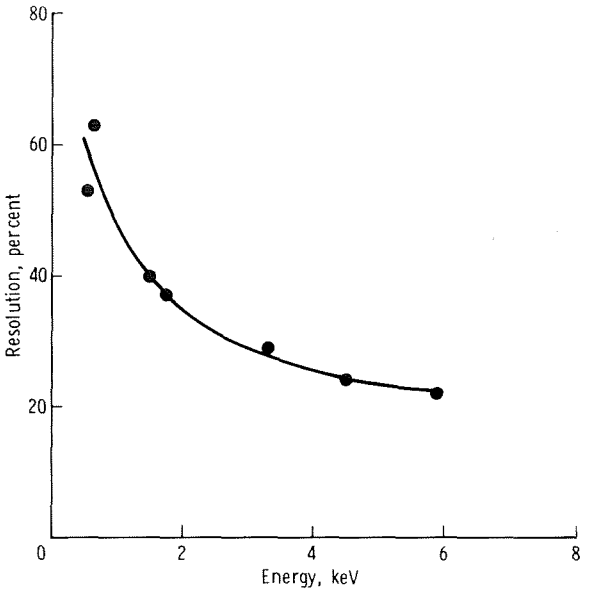

FIGURE 3-8.—Detector resolution as a function of energy calibration.

A quick in-flight calibration was provided by two radioactive sources mounted on rotary solenoids, which could be switched into the detector field of view by astronaut command. The housings for these assemblies are shown mounted to the end ribs in figure 3-3.

The flight window was installed on the detector in April 1975. The leak rate measured in vacuum was approximately 3 cm^3 Pa/min (3 cm^3 atm/min). This rate remained stable through testing, installation, and launch. No degradation was observed during the flight.

IN-FLIGHT ANOMALIES

The X-ray experiment was activated together with the other scientific instrument bay experiments approximately 35 hours after launch. Several minutes after the initial activation and calibration, an excessively high count rate was noted in the lowest spectral channels. This pattern of several minutes of normal operation followed by a period of high count rates was observed several times during the mission. The problem apparently was caused by a high-voltage breakdown.

Problems with high-voltage breakdown in proportional counters have been evident in all programs using these detectors. In addition to the usual problems of component failures and potting breakdowns, the gas gain region of the detector amplifies any discharge or breakdown caused by sharp points, metal chips, or inadequate spacing of elements. The following paragraphs give a brief operating history for the flight.

The X-ray experiment was operated on day 5 during the raster scan for the Extreme Ultraviolet Survey (EUV) Experiment. The count rates went full scale, and a gas purge was scheduled in anticipation of a possible instrument problem. After purging, the instrument was operated on the sixth day of flight, and 25 minutes of satisfactory data were obtained before the problem reappeared. On day 7, a test was performed in which the instrument was operated with the high voltage on for 2 minutes and then off for 2 minutes. The instrument operated properly for approximately 3 of the 5 minutes during which the high voltage was on. The experiment operation procedure for day 8 was revised to incorporate the 2-minute-on mode of operation, and at least 30 more minutes of satisfactory data were obtained.

On days 8 and 9, an engineering test was performed in an attempt to determine the cause of the instrument malfunction. At the end of the data take on day 8, the instrument was left in a "contingency powerdown" mode, which evacuated the gas volume of the detector. The detector was allowed to pump down to a hard vacuum overnight, and, on day 9, the high voltage was turned on with no gas in the detector. No counts at all were observed for 30 minutes or longer. This result indicated that the malfunction occurred in the gas gain volume of the detector. High-voltage potting, power supplies, and the other high-voltage components external to the gas volume of the detector were thus eliminated as possible causes of the malfunction.

The high voltage was turned off, the detector gas volume was refilled to a nominal pressure of 110 kN/m^2 (1.1 atm), and the high voltage was activated again. The detector malfunction reappeared in approximately 2 minutes, thus reaffirming the conclusion that the malfunction occurred in the gas volume of the detector.

The available data are currently being interpreted to hopefully obtain a better understanding of this malfunction. Several hypotheses have been suggested, and some laboratory tests may be needed to determine whether the characteristics of the problem can be reproduced. At present, however, no simple hypothesis convincingly explains both the intermittent nature and the preponderance of low-energy spectral counts.

Another instrumental anomaly occurred during the flight when a calibration source stuck in the field of view of the detector. The problem first occurred during the initial activation on July 21. The calibration source retracted after several momentary applications of power by the astronauts; however, the source was observed in the field of view again several orbits later, apparently because of inadvertent crew operations. No further efforts were made to dislodge the source because of the astronaut workload and the number of changes that would have been required in the Flight Plan.

In contrast to the high-voltage breakdown, the calibration source was viewed as a relatively minor problem. In analyzing the data, most of the X-ray counts caused by the calibration source can be subtracted because they occur in a narrow spectral range. (The source was iron-55 (^{55}Fe), which emits Mn_K X-rays at an energy of 5.9 keV.) The subtraction, however, does introduce some additional statistical uncertainties into the results.

OBSERVATIONS AND RESULTS

In spite of the instrumental problems encountered, several important observations were made with the Apollo-Soyuz X-ray instrument. Spectra of sources were obtained, regions of enhanced emission in the X-ray background were detected, and a new X-ray pulsar was detected. Thus, all the original objectives were met, although in a limited way, and the capabilities of a large-area X-ray detector with wide spectral and timing capabilities combined with a very flexible spacecraft system were effectively demonstrated. In the following subsections, the results of the most important observations are discussed in detail for each of the sources.

SMC X-1

The source SMC X-1 was first discovered in a rocket flight (ref. 3-1) and then found to be a binary system in *Uhuru* satellite data (ref. 3-2). The binary period is 3.9 days. An optical identification has been made with a BO supergiant in the Small Magellanic Cloud (SMC). It is believed that X-rays are produced in such binary systems when matter flows from a star (such as a supergiant) onto an unseen, compact companion (i.e., a white dwarf, a neutron star, or a black hole). In several instances, a neutron star is present and its rotation produces a pulsed modulation of the X-ray emission. One of the principal reasons for the Apollo-Soyuz observation was to search for such pulsed emission.

The Apollo observation was made at 18:50 UT on July 20, 1975. The detector was scanned toward the source by a spacecraft maneuver at a rate of 0.5° sec^{-1} yielding 30 seconds of off-source background data. The detector was pointed to within 1° of SMC X-1 for approximately 300 seconds. However, only the first 190 seconds of data are useful because the high-voltage breakdown problem occurred during the latter part of this period. The data were searched for periodicities both by Fourier analysis techniques and by folding the data modulo the suspected periods. A 0.7157-second period was detected. The pulse profiles obtained by folding the data modulo this period are shown in figure 3-9. Each bin represents the superposition of 265 36-millisecond data accumulations, and the data are displayed twice to show two full periods. The 1.6- to 7-keV data show a clear double-pulse structure with both peaks nearly equal in intensity. The off-source background is 393 counts/sec, so there is a substantial rate (400 counts/sec) from the source that is not pulsed. The pulsed fraction, or ratio of pulsed to unpulsed intensity, is 25 to 30 percent at 1.6 to 7 keV. At the lower energies (0.6 to 1.6 keV), the characteristics change dramatically. No pulsations were detected with an upper limit on the pulsed fraction of 10 percent.

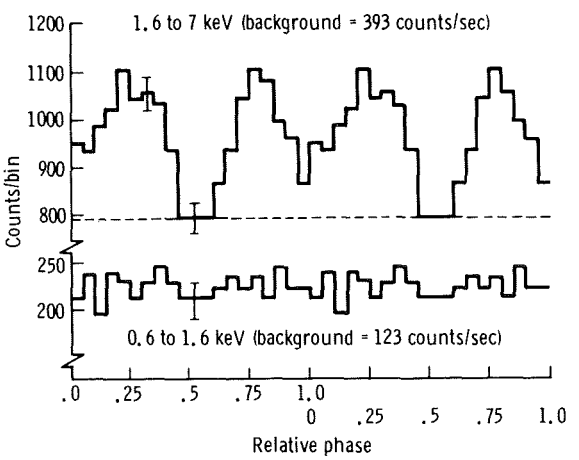

FIGURE 3-9.—Pulse profiles obtained by folding the data modulo the 0.7157-second period. The data are plotted twice to show the full profile. The dashed line indicates the estimated level of continuous emission.

A detailed spectrum of SMC X-1 was obtained and is shown in figure 3-10. The data are "best fit" by the following power law incorporating absorption by interstellar material.

$$\frac{dN}{dE} = 0.04E^{-0.8\pm0.1}\left[\exp -\sigma(E)\, N_H\right] \qquad (3\text{-}2)$$

where the interstellar hydrogen column density N_H is in the range of 0 to 2×10^{21} atoms/cm^2 and σ is the energy-dependent attenuation cross section per hydrogen atom. This spectrum is consistent with that found by the Orbiting Solar Observatory 7 (OSO-7) hard X-ray experiment (ref. 3-3) in the energy range 7 to 35 keV.

The Small Magellanic Cloud is a small galaxy 63 kpc (1 pc = 3 light-years) away from the Milky Way. At this distance, the observed X-ray luminosity of SMC X-1 is approximately 3×10^{31} J/sec (3×10^{38} ergs/sec), making it the most luminous binary X-ray source. The pulsations detected by the Apollo experiment have a period of 0.7157 second, making the SMC X-1 the binary source with the shortest pulsing period. The regular pulsations also indicate that the compact member is a rotating neutron star. Further observations of the pulsations will enable an orbital Doppler shift to be measured, which in turn will yield an accurate mass for the neutron star. Observations of long-term pulse period decreases will yield information on the transfer of angular momentum in the accretion process.

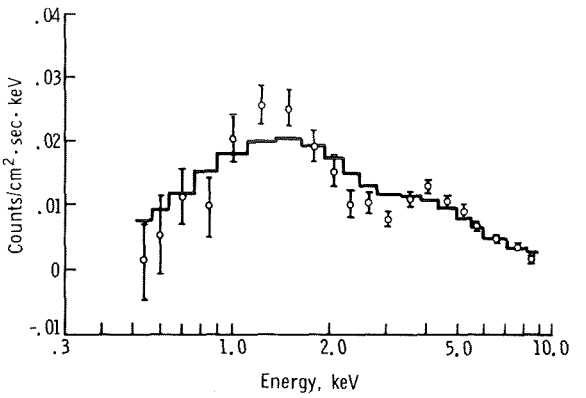

FIGURE 3-10.—The X-ray spectrum of SMC X-1. The solid line is the "best fit" power law model described in equation (3-2).

Extended Low-Energy Sources

In spite of the limited coverage obtained, at least two important observations of extended structure in the soft X-ray background were obtained. Both regions were observed to be brighter than their surroundings in the 0.6- to 2-keV band. No such enhancement was seen in the 0.18- to 0.28-keV band, probably because the regions lie close to the galactic plane where the interstellar medium absorbs the lower energy X-rays.

The first such region observed was in the constellation Centaurus. A comparison of the 0.6- to 2-keV count rate with that in adjacent regions indicates an excess of 0.084 count/cm^2 · sec. The position of maximum intensity is within 1° of a known radio supernova remnant ($\alpha = 14^h39^m, \delta = -62°15'$; ref. 3-4), and it is suggested that this same object is also the source of the X-ray emission. The regions scanned and the location of the supernova remnant are shown in figure 3-11. The distance to the supernova remnant is estimated to be 2.5 kpc, implying an X-ray luminosity of 2×10^{28} J/sec (2×10^{35} ergs/sec). The distance is consistent with the lack of observed 0.18- to 0.28-keV X-rays, and the luminosity and diameter are consistent with a remnant similar in age (10^4 years) and total energy to the Cygnus Loop.

The X-ray spectrum of this source is shown in figure 3-12. The spectrum is best accounted for by bremsstrahlung from a hot plasma at a temperature of 3×10^6 K with an interstellar hydrogen column density of 5×10^{21} atoms/cm^2.

A second extended source was observed in the constellation Cygnus. It was observed previously on a rocket flight (ref. 3-5) and was designated Cyg X-6. However, because of the Apollo-Soyuz observation and another NRL rocket observation, the source was recently shown to be extended. It does not coincide with any known radio or optical supernova remnant and, in fact, is not circular in shape but rather an elongated 1° by 8° filament. The spectrum, shown in figure 3-13, is remarkably similar to that found for the Centaurus supernova remnant. The best fit is for a hot plasma at 3×10^6 K with an intervening hydrogen column density of 8.5×10^{21} atoms/cm^2, suggesting again that the source is at least 2 kpc away.

The nature of Cyg X-6 is of considerable interest. The elongated shape suggests that it is not a single supernova remnant. It is possible that Cyg

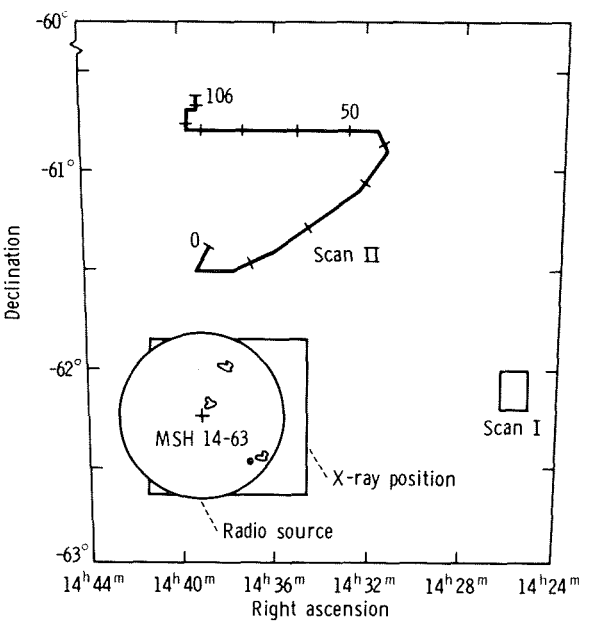

FIGURE 3-11.—Map of the region MSH 14-63 showing the Apollo scans. The best estimate of the X-ray source position is indicated. The small patches inside the remnant represent the locations of optical filaments, and the dot near the southwest rim indicates the location of the strongest continuum radio emission. Scan II is divided into time periods from 0 to 106 seconds.

X-6 is an example of an intersecting chain of remnants of the type predicted theoretically by Cox and Smith (ref. 3-6). They show that such chains are likely to occur, given the known frequency of supernova explosions and a plausible model for their evolution. When remnants do intersect, the newer one will reheat the older remnant, thus extending its X-ray-emitting lifetime.

If the minimum distance to the source suggested by the spectrum is correct, then the 1° by 8° structure is enormous, covering projected distances of 35 by 300 pc. Because the 8° (300 pc) extension is almost perpendicular to the galactic plane, it extends far above the 75- to 100-pc scale height of the neutral hydrogen disk. Such large hot plasma structures may be quite important both as a source of plasma that produces the soft X-ray background and as a means of redistributing that plasma into the galactic halo from its principal source in supernova events which occur primarily inside the neutral hydrogen disk.

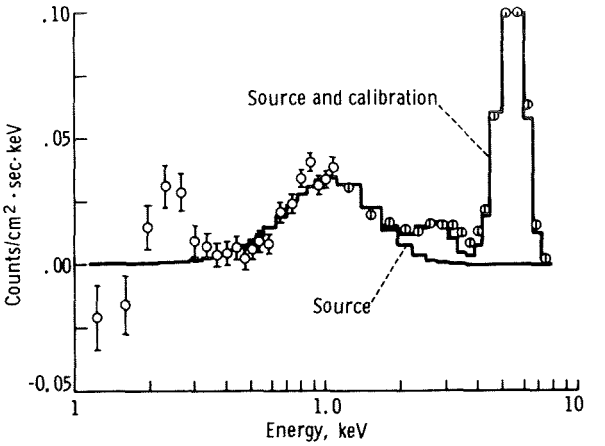

FIGURE 3-13.—The X-ray spectrum of Cyg X-6. The solid lines are the "best fit" thermal bremsstrahlung model described in the text. Top line shows the theoretical spectrum with the addition of the 5.89-keV line due to the ^{55}Fe calibration source that failed to retract properly.

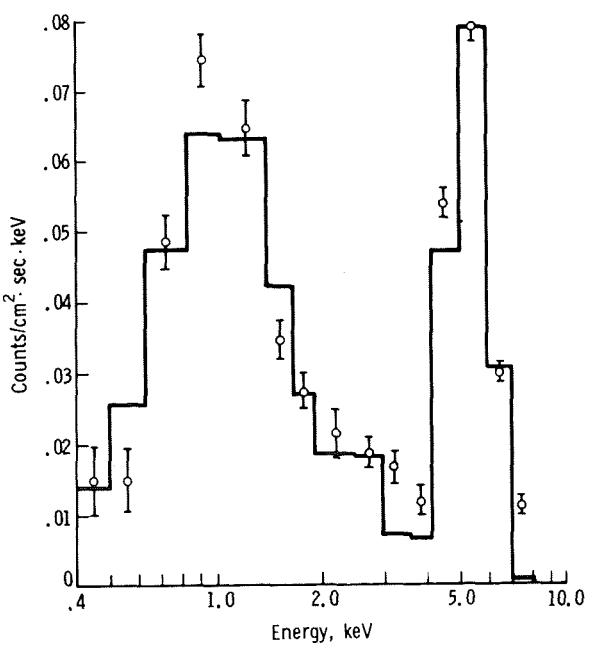

FIGURE 3-12.—The X-ray spectrum of the supernova remnant MSH 14-63. The solid line is the "best fit" thermal bremsstrahlung model (described in the text) with the addition of a 5.89-keV line due to the ^{55}Fe calibration source that failed to retract properly. (See subsection entitled "In-Flight Anomalies.")

HZ 43

The white dwarf HZ 43 was observed by both the University of California EUV telescope and the NRL X-ray instrument. The EUV measurements indicate that the star has a black-body spectrum at a temperature of approximately 110 000 K. The X-ray observation detected the source at wavelengths less than 10 nm (100 Å) (energies above 0.1 keV), which is far from the emission peak at 30 nm (300 Å). Figure 3-14 shows the X-ray count rates in three energy bands and shows the variations in the position of the source in the field of view. A significant signal was detected in both the 0.18- to 0.28-keV and 0.6- to 2-keV bands. The 0.18- to 0.28-keV count rate of $(16.2 \pm 1.8) \times 10^{-3}$ count/cm^2 • sec is consistent with the black-body spectrum observed by the EUV telescope. However, the 0.6- to 2-keV count rate of $(6.3 \pm 1.0) \times 10^{-3}$ count/cm^2 • sec is more than 100 times larger than predicted for a 110 000-K black body. The investigators searched for other sources that might have been in the field of view simultaneously and found that the coma cluster of galaxies, a known X-ray source (ref. 3-7), was seen at about 10 percent of peak response and can account for the observed 0.6- to 2-keV signal.

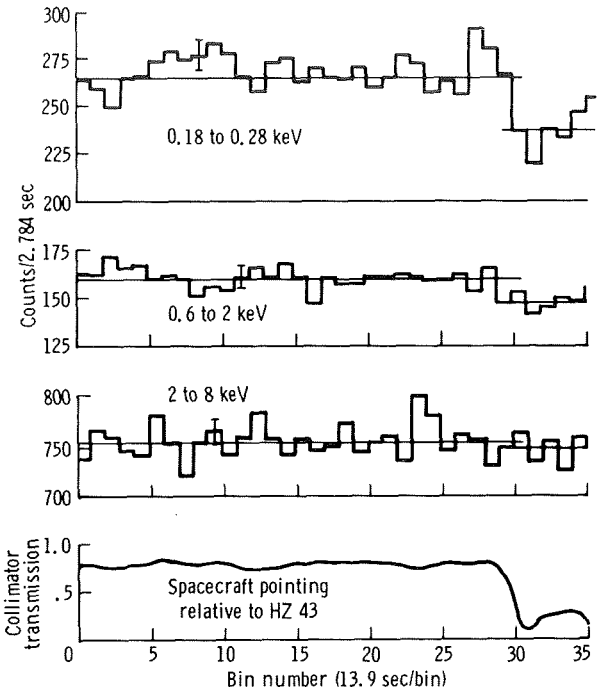

FIGURE 3-14.—Counting rates in three energy bands during the observation of HZ 43. The variation in the collimator response to the source as the spacecraft maneuvered is also shown. The horizontal lines indicate the average "on-source" rates in each energy band.

It appears, therefore, that HZ 43 has a spectrum that can be entirely accounted for by a black-body emission at 110 000 K. No evidence has been found for X-ray emission from a hot corona or for accretion at temperatures on the order of 10^6 to 10^7 K. Any such emission must be less than 5×10^{-18} J/cm^2 · sec (5×10^{-11} erg/cm^2 · sec) in the energy range 0.6 to 8 keV.

REFERENCES

3-1. Price, R. E.; Groves, D. J.; et al.: X-Rays From the Magellanic Clouds. Astrophys. J. (Letters), vol. 168, 1971, pp. L7-L9.

3-2. Schreier, E.; Giacconi, R.; et al.: Discovery of the Binary Nature of SMC-1 From *Uhuru*. Astrophys. J. (Letters), vol. 178, 1972, pp. L71-L75.

3-3. Ulmer, M. P.; Baity, W. A.; Wheaton, W. A.; and Peterson, L. E.: Observations of the Binary X-Ray Source SMC X-1 From OSO-7. Nature Phys. Sci., vol. 242, no. 121, 1973, pp. 121-123.

3-4. Downes, D.: New Radio Results on Supernova Remnants. Astronom. J., vol. 76, May 1971, pp. 305-316.

3-5. Coleman, P. L.; Bunner, A. N.; Kraushaar, W. L.; and McCammon, D.: X-Ray Observation of a New Soft Source in Cygnus. Astrophys. J. (Letters), vol. 170, 1971, pp. L47-L49.

3-6. Cox, Donald P.; and Smith, Barham W.: Large-Scale Effects of Supernova Remnants on the Galaxy: Generation and Maintenance of a Hot Network of Tunnels. Astrophys. J. (Letters), vol. 189, 1974, pp. L105-L108.

3-7. Meekins, John F.; Fritz, Gilbert; Chubb, Talbot A.; and Friedman, H.: X-Rays From the Coma Cluster of Galaxies. Nature, vol. 231, 1971, pp. 107-108.